Trajectory Optimization Formulation with Smooth Analytical Derivatives for Track-leg and Wheel-leg Ground Robots

Adwait Mane[1], Dylan Swart[2], Jason White[1], and Christian Hubicki[1]

***Abstract*— Tracks, wheels, and legs are all useful locomotion modes for Unmanned Ground Vehicles (UGVs), and ground robots that combine these mechanisms have the potential to traverse large obstacles. As robot morphologies include more degrees of freedom and obstacles become increasingly large and complex, UGVs will need to rely on motion planning algorithms to compute the joint trajectories for traversal. This article presents a trajectory optimization formulation for combined wheel-leg and track-leg UGV morphologies. One of our key contributions is a computationally efficient dynamic model of tracks, with track geometry approximated as a circulating ellipse. Using direct collocation, we formulate a model-based trajectory optimization where the objective and constraints are written in closed-form with smooth and exact derivatives for tractable computation times with existing large-scale nonlinear optimization solvers (<40 seconds). We demonstrate our optimization framework on numerous simulated planar wheel-leg and track-leg UGVs completing dynamic locomotion tasks. In the future, we plan to extend this formulation to 3D and develop contact planning algorithms for traversing large obstacles.**

I. Introduction

Unmanned Ground Vehicles (UGVs) have many forms of locomotion at their disposal, such as wheels, tracks, and legs. Each has its advantages – wheels are efficient on flat terrain, tracks provide more traction than wheels, and legs have greater maneuverability over obstacles and in cluttered environments. UGVs such as Packbot [1] and Robosimian [2] combine articulated linkages (legs) with tracks and wheels to achieve a practical compromise. As vehicle morphologies become more complex and the obstacles larger, the motion plans to traverse these obstacles become increasingly sophisticated and difficult to design (Fig. 1). Here we present a novel and computationally scalable approach to planning motions for these hybrid UGV designs, which we call wheel-leg and track-leg vehicles.

Wheel-leg UGVs are generally controlled using simple planners or are remotely controlled by a human operator. Prior work on wheel-leg UGVs has focused on statically-stable rolling motion where the primary purpose of the legs is active suspension rather than wheel lift-off [3][4]. Some recent work has demonstrated hybrid rolling and walking using reduced-order plant models [5][6]. Hybrid rolling and walking have also been demonstrated on the ANYmal robot [7] using trajectory optimization (TO). In this work, the TO problem is decomposed into wheel and base body components, and implemented using model predictive control (MPC). The wheel TO problem is formulated as a quadratic program (QP) which can be solved quickly. However, this decomposition introduces challenges. The wheels can drift away from the body while rolling and the vehicle can lose balance. Additional heuristics and cost terms are required to address these issues. Furthermore, the weights for the QP need to be tuned manually. Our approach is potentially simpler and more intuitive as these difficulties do not arise.

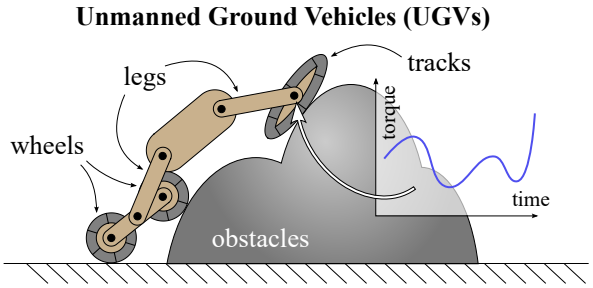

Fig. 1 As UGV morphologies become more complex, the motion plans become increasingly difficult to generate. This article proposes a motion planning framework for robot morphologies with combinations of legs, wheels, and tracks.

While tracked UGVs are capable of traversing rough terrain via simple open-loop driving, more sophisticated planning is needed for obstacles taller than the track height. A dynamic track model is necessary to use modern motion planning methods such as TO for tracks. However, current methods for modeling a circulating track are computationally expensive because the track is frequently modeled using interconnected plates [8][9]. As an alternative, tracks have been approximated using wheels for simulation [10] which reduces the obstacle-traversal capability of the simulated device. TO has been implemented on a tracked UGV for motion planning of the base body in the horizontal plane [11], which ignores the coupled dynamics between the tracks and UGV. Our formulation includes all the coupled multibody dynamics in the system.

The key contributions of our TO framework for track-leg and wheel-leg UGVs are: 1) a computationally efficient dynamic model of tracks for TO, and 2) dynamic locomotion over obstacles and uneven terrain. We approximated non-circular track geometry as an ellipse. The objective and constraints in our formulation have smooth analytical deriva-

*This work was funded by L3Harris Technologies, Inc.

[1] These authors are with the Department of Mechanical Engineering, FAMU-FSU College of Engineering, Florida State University, Tallahassee, FL 32310, USA. Corresponding author: aml9db@fsu.edu

[2] Dylan Swart is with the Department of Computer Science, Florida State University, Tallahassee, FL 32306, USA.

tives, which improves tractability of solving the TO problem and enables fast computation. We used the direct collocation formulation [12], which transcribes a TO problem to a nonlinear optimization problem. Implementing no-slip rolling contact with an ellipse in direct collocation is challenging since the elliptic arc length integral does not have a closed-form[1] solution. Our approach does not include an elliptic integral and can be generalized to contact between any two differentiable curves.

No-slip rolling contact between curved surfaces has been implemented using direct collocation [13] and using soft constraints in a dynamic programming formulation [14]. While dynamic programming methods generally work best with soft penalties, we seek a formulation for which we can specify hard constraints on the task (joint limits, torque limits, *etc.*). Rolling ellipses have also been used for locomotion of snake robots [15] and shape-changing wheels [16]. The motion plans for these systems are manually tuned. Our work offers a more automated motion planning approach for such devices.

This article is structured as follows. We first present the derivation of the dynamics and constraints, and the optimization formulation in section II: Methods. Then we present optimization results for various UGVs in section III: Results. This is followed by the Discussion and Conclusion sections. A summary video is available at [17].

II. Methods

Here we describe our direct collocation formulation for track-leg and wheel-leg vehicles. First, we introduce the multibody dynamics formulation. Then, we introduce a formulation for circular-wheeled locomotion on ramps which can be easily extended to no-slip rolling between any two differentiable curves. Next, we introduce elliptical rolling dynamics, tackling the difficulty of elliptic arc length integrals. Finally, we derive the dynamics of tracked locomotion by modeling the kinetic energy of the circulating track.

For notation, scalars are italic (x, y, L), and vectors and matrices are bold and upright ($\mathbf{q}$, $\boldsymbol{\lambda}$, $\mathbf{A}$).

A. Dynamics formulation

We used Lagrange's equations with holonomic constraints [18] to derive the dynamic equations of motion

$$\frac{\mathrm{d}}{\mathrm{d}t}\left(\frac{\partial L}{\partial \dot{\mathbf{q}}}\right)^{\top} - \left(\frac{\partial L}{\partial \mathbf{q}}\right)^{\top} = \mathbf{u} + \boldsymbol{\Gamma} \tag{1}$$

where t is time, $\mathbf{q}$ and $\dot{\mathbf{q}}$ are the position and velocity, L is the Lagrangian, $\mathbf{u}$ is the actuator input, and $\boldsymbol{\Gamma}$ is the constraint force.

Let $\mathbf{h}(\mathbf{q}) = 0$ denote the holonomic constraints in position form, and $\mathbf{A}(\mathbf{q}) = \partial \mathbf{h}(\mathbf{q})/\partial \mathbf{q}$ denote the constraint Jacobian. These constraints can be written in velocity form as

$$\frac{\mathrm{d}\mathbf{h}(\mathbf{q})}{\mathrm{d}t} = \frac{\partial \mathbf{h}(\mathbf{q})}{\partial \mathbf{q}}\dot{\mathbf{q}} = \mathbf{A}(\mathbf{q})\dot{\mathbf{q}} = 0 \tag{2}$$

[1]Closed-form (or analytical) means an expression that can be written in terms of elementary functions and operations i.e. basic arithmetic, logarithms and rational exponents, and trigonometric functions.

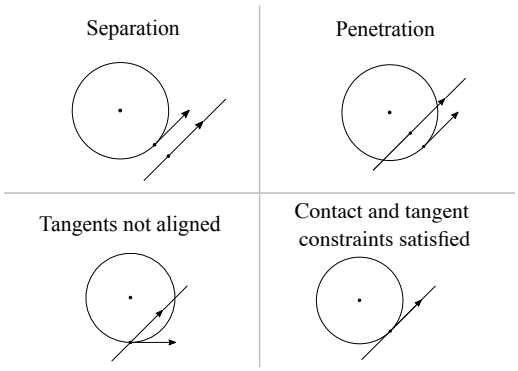

Fig. 2 **Contact and tangent constraints for rolling.** These constraints are violated when separation or penetration occurs, or when the tangents are not aligned.

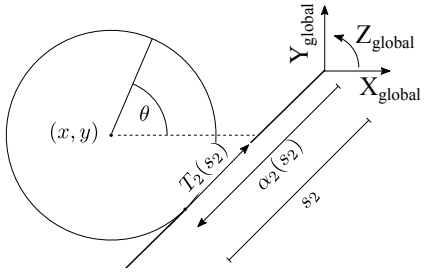

Fig. 3 **Wheel rolling without slip on a ramp: global frame.** We developed a formulation that can easily be extended to no-slip rolling between any two differentiable curves.

where $\mathbf{A}(\mathbf{q})\dot{\mathbf{q}} = 0$ is called the Pfaffian form. $\boldsymbol{\Gamma}$ can be obtained using

$$\boldsymbol{\Gamma} = \mathbf{A}(\mathbf{q})^{\top}\boldsymbol{\lambda} \tag{3}$$

where $\boldsymbol{\lambda}$ represents the Lagrange multipliers. These equations of motion are used as constraints in the direct collocation optimization.

The terms n_q and n_{DoF} denote the number of coordinates and degrees of freedom. We used non-minimal coordinates, *i.e.* $n_q > n_{DoF}$, as these naturally provide expressions for the constraint forces through Lagrange's method. The constraint forces $\boldsymbol{\Gamma}$ include the normal and tangential friction forces for no-slip rolling constraints, and their expressions can be used to apply friction cone constraints.

B. Wheel rolling without slip on a ramp

No-slip rolling between two differentiable curves is governed by the following general principles:

1) Arc lengths traversed by the contact points along the two curves must be equal.
2) Tangents at the contact points on the two curves must be aligned.
3) The two curves must maintain contact *i.e.* no separation or penetration.

We used these principles to derive the constraints for a wheel rolling without slip on a ramp. The contact and tangent constraints for this case are illustrated in Fig. 2.

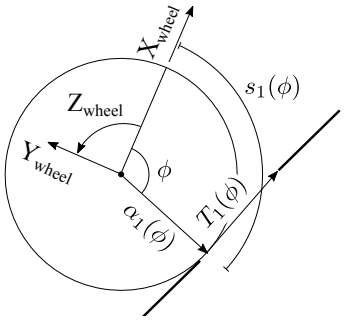

Fig. 4 **Wheel rolling without slip on a ramp: body-fixed frame.** (X_{wheel}, Y_{wheel}, Z_{wheel}) is a body-fixed frame which moves with the wheel.

We define the coordinates $\mathbf{q} = \begin{bmatrix} x & y & \theta & \phi & s_2 \end{bmatrix}^\top$. Fig. 3 shows the quantities defined in the global frame. x, y, and θ are the position and orientation of the wheel, $\boldsymbol{\alpha_2}$ and $\mathbf{T_2}$ are the contact point and tangent vector on the ramp, and s_2 is the arc length traversed along the ramp. Fig. 4 shows the quantities defined in the wheel body-fixed frame. $\boldsymbol{\alpha_1}$ and $\mathbf{T_1}$ are the contact point and the tangent vector on the wheel. We used the contact angle ϕ in the body-fixed frame to calculate the arc length s_1 traversed along the wheel. The global orientation θ can be used to calculate the arc length traversed along the wheel, however this only works for a constant slope ramp. Using ϕ allows us to generalize the terrain from a ramp to any differentiable function, which is ongoing work.

The resulting constraint expressions are

$$\mathbf{h}(\mathbf{q}) = \begin{bmatrix} r_1(\phi - \phi_0) - (s_2 - s_{2,0}) \\ \mathbf{R}(\theta)\mathbf{T_1}(\phi) \cdot \mathbf{T_2}(s_2) \\ \mathbf{c} - \boldsymbol{\alpha_2}(s_2) + \mathbf{R}(\theta)\boldsymbol{\alpha_1}(\phi) \end{bmatrix} = 0 \tag{4}$$

where r_1 is the wheel radius, ϕ_0 and $s_{2,0}$ represent the initial contact point, $\mathbf{R}(\theta)$ is the rotation matrix used to transform vectors from the wheel body-fixed frame to the global frame, and $\mathbf{c} = \begin{bmatrix} x & y \end{bmatrix}^\top$. The first expression is the arc length constraint, the second is the tangent constraint, and the third is the contact constraint.

The Lagrangian is

$$L = \frac{m(\dot{x}^2 + \dot{y}^2)}{2} + \frac{I\dot{\theta}^2}{2} - mgy \; . \tag{5}$$

The equations of motion were derived using (1), (2), and (3) with $\boldsymbol{\lambda} = \begin{bmatrix} \lambda_1 & \lambda_2 & \lambda_3 & \lambda_4 \end{bmatrix}^\top$, and $\mathbf{u} = \begin{bmatrix} 0 & 0 & u & 0 & 0 \end{bmatrix}^\top$, *i.e.* only θ is actuated.

C. Ellipse rolling without slip on flat terrain

We approximated the geometry of a circulating track as an ellipse. The rolling ellipse model derived in this section is a component of the circulating track model derived in section II-D. The coordinates of the rolling ellipse are $\mathbf{q} = \begin{bmatrix} x & y & \theta \end{bmatrix}^\top$ as shown in Fig. 5. While a simple formula exists for the arc length of a circle, there is no closed-form solution for the elliptic arc length integral. Therefore, a different approach is required to derive the no-slip constraints.

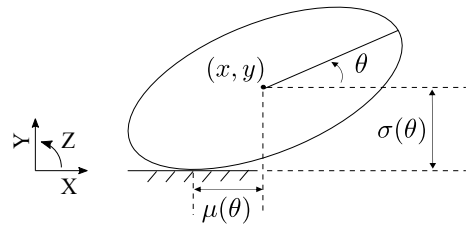

Fig. 5 **Ellipse rolling without slip on flat terrain.** The traversed arc length needs to be computed for rolling. Since the elliptic arc length integral does not have an analytical solution, we used the velocity-form of the holonomic no-slip constraints which have analytical expressions.

We begin by defining the position of the center [19] as shown in Fig. 5:

$$\sigma(\theta) = \sqrt{a^2 \sin^2(\theta) + b^2 \cos^2(\theta)} \tag{6}$$

$$\mu(\theta) = (a^2 - b^2)\frac{\sin(\theta)\cos(\theta)}{\sigma(\theta)} \tag{7}$$

where a and b are the ellipse major and minor axes lengths. No-slip rolling constraints are holonomic since they constrain the system pose[2]. For the simple case of a circle of radius r rolling on flat terrain, these constraints are

$$\mathbf{h}(\mathbf{q}) = \begin{bmatrix} x + r\theta \\ y - r \end{bmatrix} = 0 \; . \tag{8}$$

Due to non-zero eccentricity, the equivalent expressions for an ellipse are

$$\mathbf{h}(\mathbf{q}) = \begin{bmatrix} x + \int \sigma(\theta) \; \mathrm{d}\theta \\ y - \int \mu(\theta) \; \mathrm{d}\theta \end{bmatrix} = 0 \tag{9}$$

A detailed derivation of these expressions is provided in [19]. Similar to the elliptic arc length integral, there are no closed-form solutions for $\int \sigma(\theta)\mathrm{d}\theta$ and $\int \mu(\theta)\mathrm{d}\theta$. Therefore it is challenging to use them in trajectory optimization. We resolved this difficulty by using the velocity form of (9):

$$\frac{\mathrm{d}\mathbf{h}(\mathbf{q})}{\mathrm{d}t} = \begin{bmatrix} \dot{x} + \sigma(\theta)\dot{\theta} \\ \dot{y} - \mu(\theta)\dot{\theta} \end{bmatrix} = 0 \tag{10}$$

The $\mathbf{A}(\mathbf{q})$ matrix was obtained by writing (10) in Pfaffian form $\mathbf{A}(\mathbf{q})\dot{\mathbf{q}} = 0$:

$$\begin{bmatrix} 1 & 0 & \sigma(\theta) \\ 0 & 1 & -\mu(\theta) \end{bmatrix} \begin{bmatrix} \dot{x} \\ \dot{y} \\ \dot{\theta} \end{bmatrix} = 0$$

$$\Rightarrow \mathbf{A}(\mathbf{q}) = \begin{bmatrix} 1 & 0 & \sigma(\theta) \\ 0 & 1 & -\mu(\theta) \end{bmatrix}. \tag{11}$$

[2]These holonomic constraints are different from the nonholonomic constraint that arises in 3D rolling without slip. The 3D nonholonomic constraints restrict lateral velocity, which is linear z velocity for the ellipse presented here.

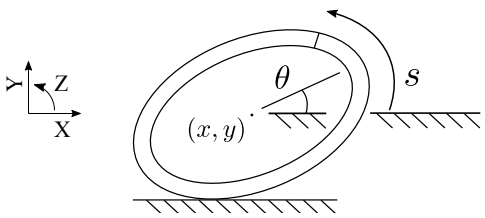

Fig. 6 **Tracked locomotion without slip on flat terrain.** Our formulation includes a dynamic model of the track. Note that positive track circulation (s) causes negative net CoM horizontal motion (x).

Using Lagrange multipliers $\boldsymbol{\lambda} = \begin{bmatrix}\lambda_1 & \lambda_2\end{bmatrix}^\top$ the constraint forces were computed as

$$\boldsymbol{\Gamma} = \mathbf{A}(\mathbf{q})^\top \boldsymbol{\lambda} = \begin{bmatrix} \lambda_1 \\ \lambda_2 \\ \sigma(\theta)\lambda_1 - \mu(\theta)\lambda_2 \end{bmatrix}. \tag{12}$$

The actuator input is $\mathbf{u} = \begin{bmatrix}0 & 0 & u\end{bmatrix}^\top$ *i.e.* only θ is actuated and the Lagrangian is identical to (5). The equations of motion were obtained after substituting into Lagrange's equations (1):

$$\begin{bmatrix} m\ddot{x} \\ m\ddot{y} + mg \\ I\ddot{\theta} \end{bmatrix} = \begin{bmatrix} \lambda_1 \\ \lambda_2 \\ \sigma(\theta)\lambda_1 - \mu(\theta)\lambda_2 + u \end{bmatrix}. \tag{13}$$

D. Tracked locomotion without slip on flat terrain

Here we extend the rolling ellipse model to a circulating elliptical track. The coordinates are $\mathbf{q} = \begin{bmatrix}\beta & y & \theta & s\end{bmatrix}^\top$ (Fig. 6) where β is the horizontal displacement of the center of mass (CoM) due to rolling and s is the track circulation distance. While the rolling ellipse is a single DoF system, the tracked ellipse has two DoFs - the body roll θ and track circulation s. The net horizontal position of the CoM is $x = \beta - s$ *i.e.* positive track circulation s causes negative net CoM horizontal motion x.

The Lagrangian is

$$L = \frac{1}{2}m(\dot{\beta}^2 + \dot{y}^2) + \frac{1}{2}I_1\dot{\theta}^2 + \frac{1}{2}I_2\dot{s}^2 - mgy \tag{14}$$

where I_1 is the rotational inertia of the ellipse and I_2 is the inertia of the track. The first two terms in L are the kinetic energy due to body roll and the third term is the kinetic energy due to track motion. This third term allows us to model the dynamics of the track.

The constraints for rolling without slip are similar to (10) with $\dot{x}$ replaced by $\dot{\beta}$ since track circulation does not directly cause rolling:

$$\frac{\mathrm{d}\mathbf{h}(\mathbf{q})}{\mathrm{d}t} = \begin{bmatrix} \dot{\beta} + \sigma(\theta)\dot{\theta} \\ \dot{y} - \mu(\theta)\dot{\theta} \end{bmatrix} = 0 \tag{15}$$

Writing the above constraints in Pfaffian form $\mathbf{A}(\mathbf{q})\dot{\mathbf{q}} = 0$ gives us

$$\mathbf{A}(\mathbf{q}) = \begin{bmatrix} 1 & 0 & \sigma(\theta) & 0 \\ 0 & 1 & -\mu(\theta) & 0 \end{bmatrix}. \tag{16}$$

Using $\boldsymbol{\lambda} = \begin{bmatrix}\lambda_1 & \lambda_2\end{bmatrix}^\top$ we get the constraint forces:

$$\boldsymbol{\Gamma} = \mathbf{A}(\mathbf{q})^\top \boldsymbol{\lambda} = \begin{bmatrix} \lambda_1 \\ \lambda_2 \\ \sigma(\theta)\lambda_1 - \mu(\theta)\lambda_2 \\ 0 \end{bmatrix}. \tag{17}$$

The only input to the system is applied to the track DoF s. The θ and s coordinates are both relative to the global frame. Therefore, based on the physics of the body to track joint, an equal and opposite torque is applied to θ. Thus, the actuator input is $\mathbf{u} = \begin{bmatrix}0 & 0 & -u & u\end{bmatrix}^\top$.

Finally, we obtain the equations of motion by substituting L, $\boldsymbol{\Gamma}$, and $\mathbf{u}$ into (1):

$$\begin{bmatrix} m\ddot{\beta} \\ m\ddot{y} + mg \\ I_1\ddot{\theta} \\ I_2\ddot{s} \end{bmatrix} = \begin{bmatrix} \lambda_1 \\ \lambda_2 \\ \sigma(\theta)\lambda_1 - \mu(\theta)\lambda_2 - u \\ u \end{bmatrix}. \tag{18}$$

E. Multibody framework

We developed a framework in Matlab that creates wheel-leg and track-leg UGVs. The user defines the UGV morphology (any planar multibody tree structure), masses, and rotational inertias using a Unified Robotics Description Format (URDF) file. The framework symbolically computes the dynamic constraints (*i.e.* equations of motion) for the trajectory optimization using the derivations described in sections II-A to II-D. The user can also specify actuator placement and bounds, joint limits, and contact (*i.e.* non-penetration and non-separation) between the bodies and the terrain. The terrain and obstacles can be represented using piecewise line segments.

F. Direct collocation formulation

The dynamic model and the rolling constraints are included in a direct collocation optimization [12], which takes the form:

$$\begin{aligned} &\min_{\mathbf{z},\boldsymbol{\lambda},\mathbf{u}} J(\mathbf{z}, \boldsymbol{\lambda}, \mathbf{u}) \\ \text{s.t.} \quad &\dot{\mathbf{z}} = \mathbf{f}(\mathbf{z}, \boldsymbol{\lambda}, \mathbf{u}) \\ &\mathbf{g}(t, \mathbf{z}, \boldsymbol{\lambda}, \mathbf{u}) \leq 0 \end{aligned} \tag{19}$$

where J is the objective, $\mathbf{z} = [\mathbf{q}, \dot{\mathbf{q}}]^\top$ is the state, $\boldsymbol{\lambda}$ is the Lagrange multiplier, $\mathbf{u}$ is the control input, $\mathbf{f}$ is the dynamic model in first-order form, and $\mathbf{g}$ contains all the path constraints (such as rolling constraints). The decision variables in our optimization are $\mathbf{z}$, $\boldsymbol{\lambda}$, $\mathbf{u}$, and acceleration (slack variable) [12]. By design of the presented formulation, $\mathbf{f}$ and $\mathbf{g}$ are closed-form analytical expressions with smooth derivatives, enabling fast trajectory optimization with existing nonlinear optimization solvers.

III. Results

We implemented this framework on a variety of systems with tracks, wheels, and legs. Videos of the results are available at [17] and Table I provides a summary. We used arbitrary geometric and inertial parameters since the focus of this work is to demonstrate the formulations for rolling

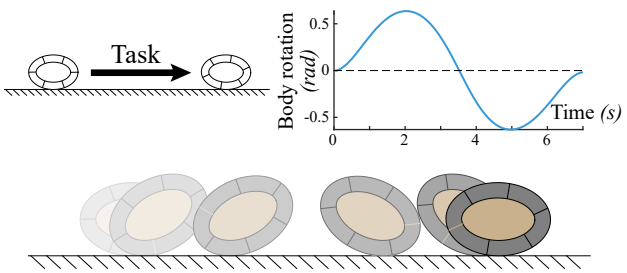

Fig. 7 **Tracked ellipse.** The task to move to the right using track actuation, starting and ending at rest. This optimization result shows the dynamic coupling between the track and the body.

and tracked locomotion. Gravity = 9.81 m/s^2, body masses are in the 0.5 to 1 kg range, all bodies are assumed to be homogeneous for rotational inertia calculations, and lengths are on the order of 1 m.

	No. of nodes	Objective	Computation time (s)
Tracked ellipse	101	$\int_0^T \|\mathbf{u}\|_2 \, dt$	0.9
Tracked double pendulum	51	0	0.4
Tracked bicycle	101	$\int_0^T \|\mathbf{v}_{base}\|_2 \, dt$	38.5
Wheeled bicycle	101	$\int_0^T \|\mathbf{u}\|_2 \, dt$	3.8
Articulated UGV	51	0	35.1

TABLE I Summary of the results. $\mathbf{u}$ is the actuator input and $\mathbf{v}_{base}$ is the base translational velocity. $\|\cdot\|_2$ is the Euclidean norm.

We used the COALESCE direct collocation package [20] in Matlab with IPOPT [21] as the underlying nonlinear optimization solver. All the optimizations had a fixed time horizon. The solver converged to either an optimal or acceptable solution (tolerance = 1e-8) for all the results presented. All optimizations were performed on a Lenovo Yoga 920-13IKB laptop with an Intel Core i7-8550U processor.

We considered three types of objectives: zero, force-minimizing, and velocity-minimizing (Table I). A zero-objective optimization serves as a feasibility check: if a solution is found, then the problem is feasible. This solution is not necessarily optimal. A zero-objective was tried first for all systems. Then we tried to find locally optimal solutions using non-zero objectives. We have reported the zero-objective solutions for the tracked double pendulum and articulated UGV since the non-zero objective cases did not converge.

A. Tracked vehicles

Figs. 7 and 8 show that our formulation can be used to plan dynamic motions for underactuated tracked systems. Fig. 7 is a force-minimizing optimal solution. The task is to move 7 m to the right using track actuation, starting and ending at rest. This result shows how our formulation accounts for the track dynamics. The dynamic coupling between the body roll (θ) and track circulation (s) DoFs causes the body to counter-rotate as the track accelerates and decelerates. The feasible solution for the tracked double pendulum (Fig. 8) shows that our formulation can perform dynamic balancing. The ellipses in these examples have an eccentricity of 0.7 and major axis length of 1 m.

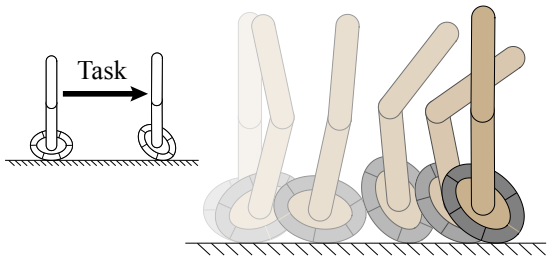

Fig. 8 **Tracked double pendulum.** This optimization shows that our formulation can perform dynamic balancing.

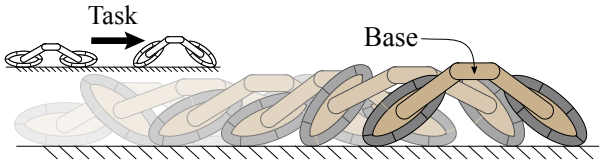

Fig. 9 **Tracked bicycle.** The task is to move to the right and raise the base while keeping it horizontal, starting and ending at rest. This optimization shows that our formulation can handle multiple contacts with track-leg vehicles.

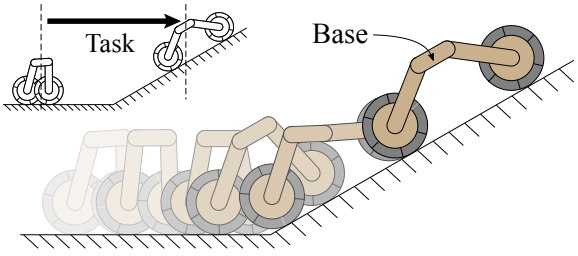

Fig. 10 **Wheeled bicycle.** The bicycle changes contact modes to complete the task, showing the ability to handle multiple contact modes.

Fig. 9 shows a velocity-minimizing optimal solution for a tracked bicycle. The task is to move 10 m to the right and lift the base by 0.6 m. The base is constrained to remain horizontal. This result demonstrates that our formulation can handle multiple contacts with track-leg vehicles. The elliptical tracks in this optimization have an eccentricity of 0.9 and major axis length of 1.5 m, which shows that the formulation can represent tracks with extreme aspect ratios.

B. Wheeled vehicles

Trajectory optimization for traversing uneven terrain is challenging due to discontinuities at contact mode transitions. A contact mode specifies which body and terrain segments are in rolling contact. In our formulation, each contact mode has a distinct constraint expression. Therefore, the constraint expressions vary with the contact mode, which introduces discontinuities. This requires a multiphase optimization approach [22] in which the constraints in each

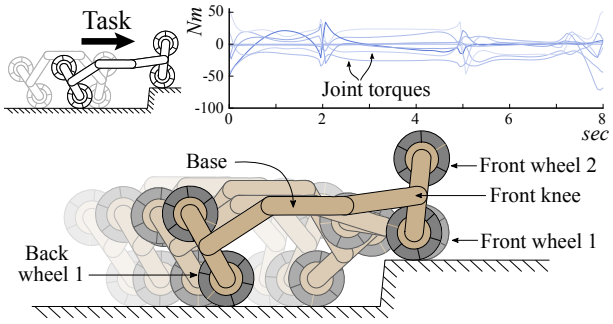

Fig. 11 **Articulated UGV climbing a step.** This optimization shows how multiple contact modes can be used in our formulation to lift the wheels and traverse obstacles.

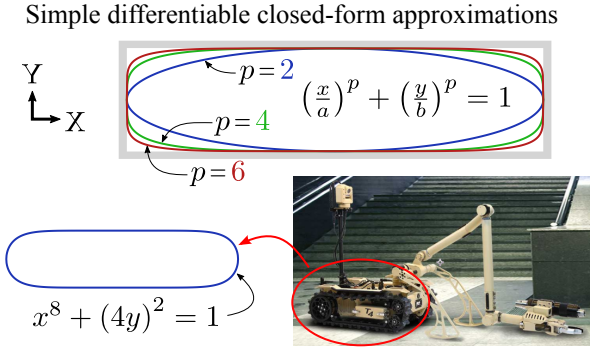

Fig. 12 Higher order ellipses can better approximate track geometry. The ellipse parameters were tuned manually. Photo credit: [23].

phase differ based on the contact mode. Boundary constraints are applied at the phase transitions to connect the state trajectories. In this work, all joint velocities were constrained to be zero at the contact mode transitions to eliminate impact forces. The contact mode sequence is currently manually scheduled as contact planning in a direct collocation framework is challenging [13].

Fig. 10 shows the ability to change contact modes. The task for the wheeled bicycle is to move 10 m to the right, and the bicycle changes contact modes to climb the ramp and perform the task. The bicycle uses three contact modes: the first has both wheels on the horizontal terrain segment, the second has one wheel each on the horizontal and ramp segments, and the third has both wheels on the ramp.

The articulated UGV example (Fig. 11) demonstrates the ability to traverse an obstacle. The UGV starts with front wheel 2 and back wheel 1 in contact with the lower terrain segment. The task is to place front wheel 1 on top of the step and then bring front wheel 2 ahead of front wheel 1 using two contact modes. The UGV rotates the front knee to achieve this task. The supplementary video [17] shows this maneuver in more detail.

IV. Discussion

Our long-term goal is to develop contact planning algorithms for track-leg and wheel-leg locomotion over large obstacles. In the present work, we used manually scheduled contact sequences, but this is impractical for locomotion on more complex terrain. Features such as uneven terrain, multiple contact modes, and wheel-lift off (*e.g.* Fig. 11) presented in this article are steps towards the long-term goal.

Tracked UGVs in the field encounter a number of challenges while traversing obstacles. The track to terrain contact patch over an obstacle can be much smaller than on flat terrain causing the UGV to sway back and forth as the track accelerates. This is similar to the counter-rotation of the tracked ellipse body in response to track acceleration (Fig. 7). We plan to extend our formulation to include obstacles represented by curved terrain, where such dynamic behaviors can play an important role.

We plan to use more realistic terrain and track geometry in the future. While the rolling ellipse formulation in section II-C is specific to flat terrain, the general principles presented in section II-B apply to no-slip rolling between any two differentiable curves. We plan to apply these general principles to locomotion on curved terrain segments and obstacles represented using polynomials. Additionally, higher order ellipses can be used to obtain more realistic track geometry (Fig. 12). Future work also includes extending this work to 3D with ellipsoid to ellipsoid rolling contact. This can accommodate more complex morphologies but also presents new challenges, such as nonholonomic constraints on the lateral velocity during rolling.

We plan to implement a more realistic no-slip regime in our framework. While the friction forces are unbounded in our current implementation, the Lagrange multipliers $\boldsymbol{\lambda}$ can be used to include friction cone constraints in the optimization. In the real world, disturbances (such as slip) and model uncertainties are inevitable. Feedback control can be used to reject such disturbances, and track reference trajectories generated by the optimization. Control strategies ranging from simple joint level proportional-integral-derivative control to more sophisticated approaches such as whole-body tracking control [24] can be used for this purpose.

V. Conclusion

We present a novel formulation for trajectory optimization of wheel-leg and track-leg UGVs. We achieved mission-tractable computation times (<40 seconds) by deriving a direct collocation formulation which casts the dynamics as constraints with smooth analytical derivatives. We demonstrated the framework with multiple simulated planar UGVs completing assorted locomotion tasks.

References

[1] B. M. Yamauchi, "Packbot: a versatile platform for military robotics," in *Unmanned ground vehicle technology VI*, vol. 5422. International Society for Optics and Photonics, 2004, pp. 228–237.

[2] B. W. Satzinger, C. Lau, M. Byl, and K. Byl, "Tractable locomotion planning for robosimian," *The International Journal of Robotics Research*, vol. 34, no. 13, pp. 1541–1558, 2015.

[3] A. Suzumura and Y. Fujimoto, "Real-time motion generation and control systems for high wheel-legged robot mobility," *IEEE Transactions on Industrial Electronics*, vol. 61, no. 7, pp. 3648–3659, 2013.

[4] W. Reid, F. J. Pérez-Grau, A. H. Göktoğan, and S. Sukkarieh, "Actively articulated suspension for a wheel-on-leg rover operating on a martian analog surface," in *2016 IEEE International Conference on Robotics and Automation (ICRA)*. IEEE, 2016, pp. 5596–5602.

[5] A. Laurenzi, E. M. Hoffman, and N. G. Tsagarakis, "Quadrupedal walking motion and footstep placement through linear model predictive control," in *2018 IEEE/RSJ International Conference on Intelligent Robots and Systems (IROS)*. IEEE, 2018, pp. 2267–2273.

[6] J. Sun, Y. You, X. Zhao, A. H. Adiwahono, and C. M. Chew, "Towards more possibilities: Motion planning and control for hybrid locomotion of wheeled-legged robots," *IEEE Robotics and Automation Letters*, vol. 5, no. 2, pp. 3723–3730, 2020.

[7] M. Bjelonic, P. K. Sankar, C. D. Bellicoso, H. Vallery, and M. Hutter, "Rolling in the deep–hybrid locomotion for wheeled-legged robots using online trajectory optimization," *IEEE Robotics and Automation Letters*, vol. 5, no. 2, pp. 3626–3633, 2020.

[8] D. Rubinstein and R. Hitron, "A detailed multi-body model for dynamic simulation of off-road tracked vehicles," *Journal of Terramechanics*, vol. 41, no. 2-3, pp. 163–173, 2004.

[9] M. McCullough, A. Khubchandani, A. Shyu, and D. Simoni, "Verification and fidelity of high mobility tracked vehicle dynamic models," *SAE Transactions*, pp. 87–104, 2006.

[10] I. Moskvin, R. Lavrenov, E. Magid, and M. Svinin, "Modelling a crawler robot using wheels as pseudo-tracks: model complexity vs performance," in *2020 IEEE 7th International Conference on Industrial Engineering and Applications (ICIEA)*. IEEE, 2020, pp. 1–5.

[11] M. Giftthaler, T. Sandy, K. Dörfler, I. Brooks, M. Buckingham, G. Rey, M. Kohler, F. Gramazio, and J. Buchli, "Mobile robotic fabrication at 1: 1 scale: the in situ fabricator," *Construction Robotics*, vol. 1, no. 1, pp. 3–14, 2017.

[12] M. Kelly, "An introduction to trajectory optimization: How to do your own direct collocation," *SIAM Review*, vol. 59, no. 4, pp. 849–904, 2017.

[13] M. Posa, C. Cantu, and R. Tedrake, "A direct method for trajectory optimization of rigid bodies through contact," *The International Journal of Robotics Research*, vol. 33, no. 1, pp. 69–81, 2014.

[14] Y. Tassa and E. Todorov, "Stochastic Complementarity for Local Control of Discontinuous Dynamics," in *Robotics: Science and Systems VI*, Matsuoka, Y and DurrantWhyte H and Neira, J, Ed., 2011, pp. 169–176.

[15] R. L. Hatton and H. Choset, "Sidewinding on slopes," in *2010 IEEE International Conference on Robotics and Automation*. IEEE, 2010, pp. 691–696.

[16] D. Mellinger, V. Kumar, and M. Yim, "Control of locomotion with shape-changing wheels," in *2009 IEEE International Conference on Robotics and Automation*. IEEE, 2009, pp. 1750–1755.

[17] A. Mane, D. Swart, J. White, and C. Hubicki, *ICRA22 Trajectory Optimization for Track-leg and Wheel-leg Robots*. YouTube, Feb 2022. [Online]. Available: https://youtu.be/-cF39_6Sj-Q

[18] R. Murray, Z. Li, S. Sastry, and S. Sastry, *A Mathematical Introduction to Robotic Manipulation*. CRC Press, 1994.

[19] R. Rostamian, "Rolling an ellipse in a vertical plane," https://www.mapleprimes.com/posts/210428-Rolling-An-Ellipse-In-A-Vertical-Plane, April 2019, accessed 2020 June 13.

[20] M. S. Jones, "Optimal control of an underactuated bipedal robot," 2014.

[21] A. Wächter and L. T. Biegler, "On the implementation of an interior-point filter line-search algorithm for large-scale nonlinear programming," *Mathematical programming*, vol. 106, no. 1, pp. 25–57, 2006.

[22] M. A. Patterson and A. V. Rao, "Gpops-ii: A matlab software for solving multiple-phase optimal control problems using hp-adaptive gaussian quadrature collocation methods and sparse nonlinear programming," *ACM Transactions on Mathematical Software (TOMS)*, vol. 41, no. 1, pp. 1–37, 2014.

[23] "T4 robotic system," https://www.l3harris.com/all-capabilities/t4-robotic-system, accessed 2021 September 14.

[24] M. Bjelonic, C. D. Bellicoso, Y. de Viragh, D. Sako, F. D. Tresoldi, F. Jenelten, and M. Hutter, "Keep rollin'—whole-body motion control and planning for wheeled quadrupedal robots," *IEEE Robotics and Automation Letters*, vol. 4, no. 2, pp. 2116–2123, 2019.